ISSN 2228-9860 eISSN 1906-9642 CODEN: ITJEA8

International Transaction Journal of Engineering, Management, & Applied Sciences & Technologies

http://TuEngr.com

Wind Load Combinations on Tall Buildings by High-Frequency Force Balance and High-Frequency Pressure Integration

Wasin Thangthong[1], Virote Boonyapinyo[1*], and Jirawat Junruang[2]

[1]*Department of Civil Engineering, Thammasat School of Engineering, Thammasat University, THAILAND.*
[2]*Department of Civil Engineering, Faculty of Engineering and Architecture, Rajamangala University of Technology Tawan-ok (Uthenthawai Campus), THAILAND.*
**Corresponding Author (Email: bvirote@engr.tu.ac.th).*

Paper ID: 13A9E

Volume 13 Issue 9

Received 12 April 2022
Received in revised form 06 June 2022
Accepted 15 June 2022
Available online 24 June 2022

Keywords:
High-frequency force balance (HFFB); Pressure integration method; AIJ; Wind tunnel test; Modal correlation coefficients; HFPI Test; HFFB test; Wind load combination; Tall building modeling; Static wind load; Wind velocity profile; Spectrum of wind; Turbulence intensity profiles; Base Moment Analysis.

Abstract

This paper presents the analysis of the modal correlation coefficient and the weighting factor for predicting wind load combinations in tall buildings under wind loads by high-frequency force balance (HFFB) and high-frequency pressure integration (HFPI) in a wind tunnel. The results of the analysis and comparisons in terms of non-dimensional aerodynamic coefficients and base moments will be presented in this study, to determine whether the pressure tap on the model surface for the HFPI test is sufficiently dense. Results show good agreement between HFFB and HFPI for overall wind loads, modal correlation coefficients and weighting factors. Wind load combinations are revisited in the framework of modeling the resultant base moments in each direction. According to the findings, the across-wind load combination by weighting factor is higher than the across-wind load combination by AIJ 2004 standard for the along-wind maximum case for buildings with an aspect ratio of 1.0. In other cases, the combination of wind loads as determined by AIJ 2004 is greater than the combination of wind loads determined by the weighting factor.

Disciplinary: Civil Engineering & Technology (Structural Engineering).

Cite This Article:

Thangthong, W., Boonyapinyo, V., and Junruang, J. (2022). Wind Load Combinations on Tall Buildings by High-Frequency Force Balance and High-Frequency Pressure Integration. *International Transaction Journal of Engineering, Management, & Applied Sciences & Technologies*, 13(9), 13A9E, 1-14. http://TUENGR.COM/V13/13A9E.pdf DOI: 10.14456/ITJEMAST.2022.173

1 Introduction

Wind load is one of the lateral loads that are important to the analysis and design of tall building structures. Wind load analysis that is both wrong and insufficient might result in structural damage. In recent decades, wind tunnel tests have been accepted industry-wide for

evaluating wind-induced structural loads and the response of tall buildings and other structures. The longest and most extensively utilized method of testing is the high-frequency force balance (HFFB). This test is based on measuring the overall wind loads acting at the base of a model in six components (three components of force and three moments). The force distributions over the height of the building require an assumption of the mean wind speed exponential coefficient. On the other hand, the high-frequency pressure integration (HFPI) test is based on the simultaneous measurement from multi-point sensing of pressure at several locations on the model surface. Simply put, assuming the pressure taps are installed with fine enough resolution throughout the building surfaces, integrating the data should yield the same result as an HFFB test. This test provides a good and realistic load distribution over the height of the buildings. The HFPI test also allows the higher mode to be considered, and the data pressure around the building can use for the prediction of cladding design.

The combination of wind load acting on tall buildings in three directions is often preferred by AIJ 2004 standard. The weighting factor for AIJ 2004 standard is based on non-correlation between along and across-wind, including along-wind and torsional. However, the correlation between across-wind and torsional is considered to be about 0.2. Alternatively, the wind load combination can be obtained from the model testing in a wind tunnel for predicting the weighting factor that takes into account the modal correlation coefficient between two modal responses and the ratio of wind forces in each axis in each angle of wind attack, which presents in this study.

2 Literature Review

Research on the determination of the overall wind load and the response of tall buildings using the HFFB method was presented by Zhou et al. (2003) and Kwon et al. (2008). This study was conducted with the HFFB method and presented the base moment analysis divided into three parts, which are mean, background and resonance parts and also show the result in terms of non-dimensional aerodynamic coefficient. In addition, this research also presents a formulation for predicting the response of the building and assumptions in distributing loads over the height of the building. Chen and Kareem (2005a) propose a framework of generalized wind force analysis for the investigation of the coupled 3D dynamic response of the structure. This framework considers the intermodal coupling of modal response components as well as the correlation between wind loads in principle loads in principle directions. Chen and Kareem (2005b) used the HFFB test to analyze the effect of overall wind loads on a coupled tall building. This framework indicates that the generalized wind force analysis can be used for any type of building geometry because it's not used an ideal fundamental mode shape like the base moment analysis. Furthermore, this approach also allows 3D coupled mode and higher modes to be considered.

Steckley et al. (1992) tested the model with the HFPI test and compared the mean base moment and dynamic base moment with the HFFB test. The result showed that both tests produced identical results. Kwon, Spence and Kareem (2014) introduce the DEDM-HRP, a new data-enabled design model for high-rise buildings propelled by pressure datasets, which smoothly integrates

synchronous pressure measurement databases with a demanding computational framework to provide a quick estimation of wind load impacts on high-rise buildings for their preliminary design.

Tamura et al. (2003) studied the effect of wind load combinations on low and mid-rise buildings by testing a rectangular model in a wind tunnel. The findings demonstrated that there was a high correlation between along-wind force and across-wind force, along-wind force and torsional moment. Asami (2000) studied the correlation coefficient for combining wind load of across-wind and torsional, and it was implemented in AIJ 2004 standard. Tamura, Kim, Kikuchi and Hibi (2013) studied wind load combination effects for low-, middle- and high-rise. The cross-correlation between wind force components is investigated using phase-plane trajectories, which is the absolute ratio of wind forces.

3 Experimental Test

3.1 Wind Tunnel Test

This study was achieved by a wind tunnel experiment on a tall building model which was carried out in the boundary-layer test section of the TU-AIT wind tunnel laboratory, Pathumthani, Thailand as shown in Figure 1(a). The dimensions of the test section are 2.5 m in width, 2.5 m in height and 25.5 m in length. To model the growth of the boundary layer, passive vortex generators in the shape of spires, brick and roughness components in the shape of pyramids were utilized at the entrance of the test area. The terrain profile employed here is representative of a typical urban terrain profile.

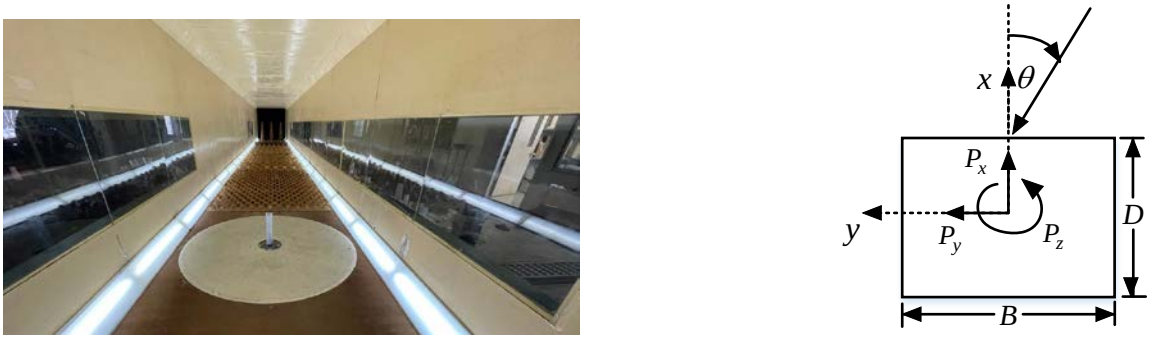

(a) (b)

Figure 1: (a) Wind tunnel (b) Angle of attack on the model

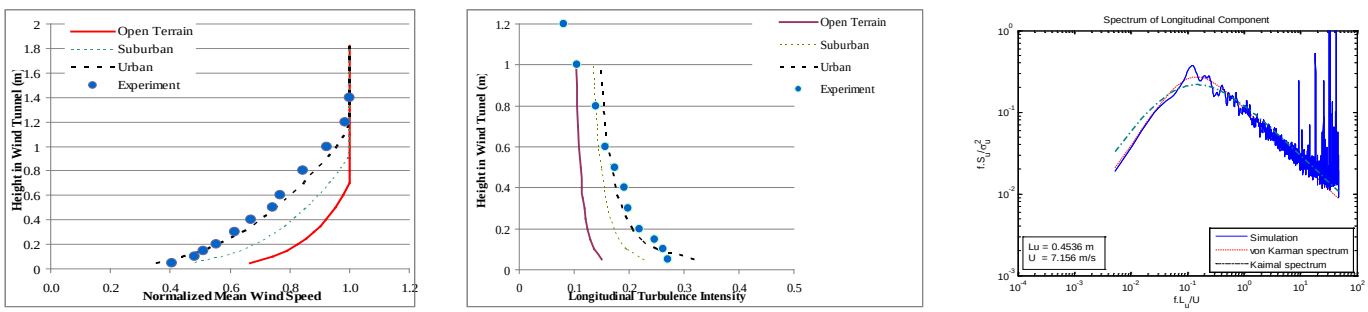

(a) (b) (c)

Figure 2: (a) Mean wind velocity profile (b) Turbulence intensity profiles (c) Spectrum of wind.

Figure 2(a) shows the mean velocity profile normalized at the reference height. Figure 2(b-c) shows the velocity spectrum and turbulence intensity profiles at the reference height. The length

scale used in this experiment was 1:400. The wind tunnel test was carried out for 36 different wind directions at an interval of 10 degrees. The direction and angle of the wind attack on the model are shown in Figure 1(b).

3.1.1 Tall Building Modeling

The building employed in this study has 40 stories with the same square cross-section of 30 m × 30 m and a story height of 4 m (Total height is 160 m) are shown in Figure 3(a). The building is modeled as an RC building with a building average density of 382 kg/m^3. The fundamental frequencies in x, y and z-direction for the buildings are 0.169 Hz, 0.169 Hz and 0.303 Hz shown in Figure 3(b). The damping ratio for each mode is assumed to be 2%.

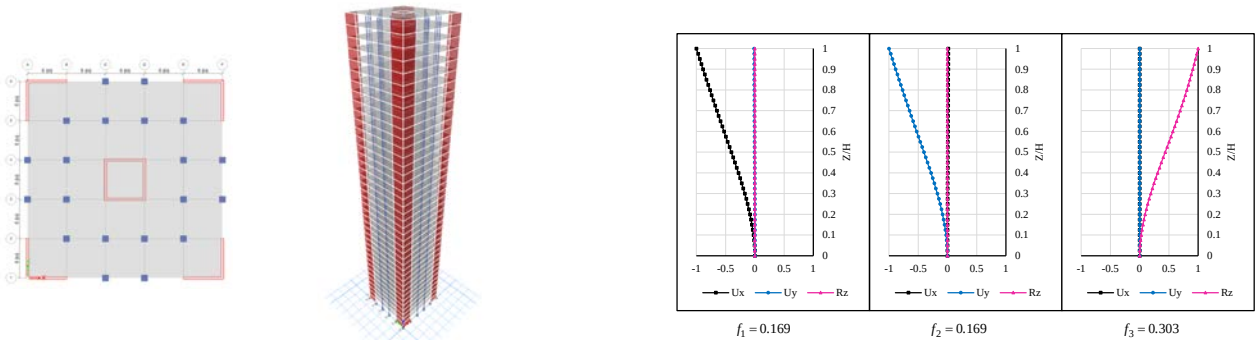

(a) (b)

Figure 3: (a) Finite element modeling (b) The fundamental vibration modes of building.

3.1.2 HFFB Test

This test uses a rigid model to conduct wind tunnel tests are shown in Figure 4(a), with the dynamic properties of the full-scale structure taken into consideration in the analysis. The JR3 multi-axis load cell was used to quantify the overall wind load at the base of the model shown in Figure 4(b). The sampling rate of wind force time history was 1,000 data/sec, and a total of 210,000 data were recorded throughout a 210-second period.

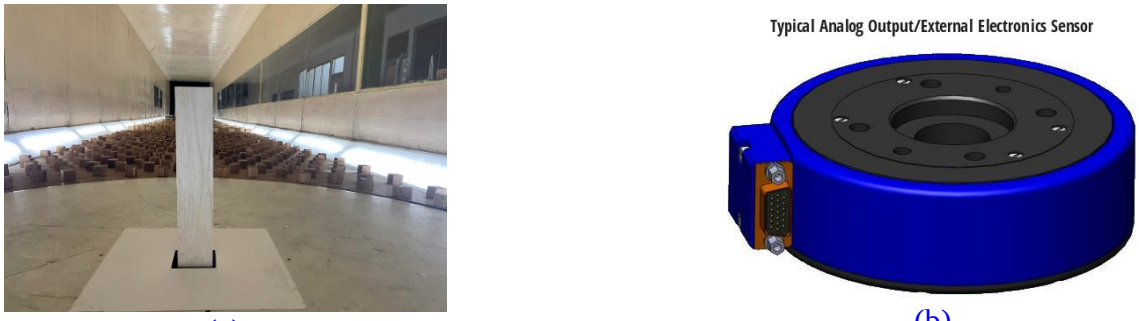

(a) (b)

Figure 4: (a) HFFB model (b) The JR3 multi-axis load cell.

3.1.3 HFPI Test

The wind pressure on the rigid acrylic model surface is measured in the HFPI test using a synchronous multi-pressure sensor system, the model includes pressure taps mounted at 9 levels and 20 points per level on the model surface, as shown in Figure 5(a-b). The sampling rate of wind pressure time history was 400 data/sec, and a total of 80,000 data were recorded throughout a 120-second period.

(a)

(b)

Figure 5: (a) HFPI model (b) The pressure sensor system

4 Analysis Framework

4.1 The Base Moment Analysis

This analysis uses the base moment of the model to investigate the result to determine the overall wind loads acting on buildings. This approach is based on an ideal fundamental mode shape with linear translation modes in x and y, the constant torsional mode in z and then applying mode shape corrections. In analysis, the torsional base moment is required for mode shape correction equal to 0.7, which was proposed by Zhou et al. (2003), Kwon et al. (2008). For the HFFB test, the base moment of the model is obtained from the test, which allows direct analysis of this method. But for the HFPI test, the pressure of the model surface is obtained from the test, which requires the pressure to be converted to the base moments of the model before analysis.

4.1.1 Mean Wind Force Coefficients

Mean wind force coefficients represent the mean base moment of the building, which can be calculated from

$$C_x = \frac{\bar{M}_{ym}(2+2\alpha_m)}{0.5\rho_m \bar{U}_{Hm}{}^2 B_m H_m{}^2} \quad (1),$$

$$C_y = \frac{\bar{M}_{xm}(2+2\alpha_m)}{0.5\rho_m \bar{U}_{Hm}{}^2 D_m H_m{}^2}(-1) \quad (2),$$

$$C_z = \frac{\bar{M}_{zm}(1+2\alpha_m)}{0.5\rho_m \bar{U}_{Hm}{}^2 B_m D_m H_m} \quad (3),$$

where C_x, C_y and C_z are mean wind force coefficients in x, y and z direction; $\bar{M}_{xm}$, $\bar{M}_{ym}$ and $\bar{M}_{zm}$ are the mean base moments of model about x, y and z axis; α_m is mean wind speed exponential coefficient; ρ_m is air density; U_{Hm} is wind velocity at top of the model; H_m, B_m and D_m are height, width and depth of the model (see Figure 2(b)).

4.1.2 RMS of Fluctuating Base Moment Coefficients

RMS of fluctuating base moment coefficients represents the background base moment of the building, this can be calculated using

$$\sigma_{cmx} = \frac{\sigma_{mx}}{0.5\rho_m \bar{U}_{Hm}{}^2 D_m H_m{}^2} \quad (4),$$

$$\sigma_{cmy} = \frac{\sigma_{my}}{0.5\rho_m \bar{U}_{Hm}{}^2 B_m H_m{}^2} \quad (5),$$

$$\sigma_{cmz} = \frac{\sigma_{mz}}{0.5\rho_m \bar{U}_{Hm}{}^2 B_m D_m H_m} \quad (6),$$

where σ_{cmx}, σ_{cmy} and σ_{cmz} are non-dimensional root-mean-square of base moment coefficients about x, y and z axis; σ_{mx}, σ_{my} and σ_{mz} are root-mean-square of the base moments of model about x, y and z-axis.

4.1.3 Power Spectrum Density of Fluctuating Base Moments

The power spectrum density of fluctuating base moments is to transform the base moment time history data into frequency domain data, which can be carried out by the Fourier transform.

4.2 The Generalized Wind Force Analysis

The generalized wind force analysis uses the force distributions over the height of the building to determine the overall wind loads acting on buildings, including the response of buildings such as displacements and accelerations. For the HFFB test, the force distributions over the height of the building are obtained from the distribution of the base moment according to the assumption of the mean wind speed exponential coefficient from Equations (9) and (10). However, for the HFPI test, multiple point synchronous sensing of pressure on the building model surface is used to calculate force distributions over the building's height.

$$M_p(t) = M_m(t_m) / \left(\lambda_p \lambda_L{}^3 \lambda_U{}^2\right) \quad (7),$$

$$P_{p_i}(t) = P_{m_i}(t_m) / \left(\lambda_p \lambda_L{}^2 \lambda_U{}^2\right) \quad (8),$$

$$P_{D,L}(z) = M_{D,L} \frac{2+2\alpha_p}{H^2} \left(\frac{z}{H}\right)^{2\alpha_p} \Delta H \quad (9),$$

$$P_T(z) = M_T \frac{1+2\alpha_p}{H} \left(\frac{z}{H}\right)^{2\alpha_p} \Delta H \quad (10),$$

where $M_p(t)$ and $M_m(t_m)$ are base moments of real building and model; λ_p is density scale; λ_L is length scale; λ_U is velocity scale; $P_{p_i}(t)$ and $P_{m_i}(t_m)$ are forces acting on the ith floor of real building and model; $P_{D,L}(z)$ is a force acting at the height z of the building in along and across wind directions; $P_T(z)$ is a force acting at the height z of the building in torsional directions; H and ΔH are the height of the building and floor-floor height of the building; α_p is mean wind speed exponential coefficient of real buildings; Subscript p and m are real building and model.

The mean and dynamic generalized wind force can be calculated from

$$\bar{Q}_j = \sum_{i=1}^{N} \left(\phi_{ijx} \bar{P}_{ix} + \phi_{ijy} \bar{P}_{iy} + \phi_{ijz} \bar{P}_{iz}\right) \quad (11),$$

$$Q_j(t) = \sum_{i=1}^{N} \left(\phi_{ijx} P_{ix}(t) + \phi_{ijy} P_{iy}(t) + \phi_{ijz} P_{iz}(t)\right) \quad (12),$$

where $\bar{Q}_j$ and $Q_j(t)$ are mean and dynamic generalized wind force of jth mode; $\bar{P}_{ix}$, $\bar{P}_{iy}$ and $\bar{P}_{iz}$ are mean force acting on the ith floor of the building in x, y and z direction; ϕ_{ijx}, ϕ_{ijy} and ϕ_{ijz} are jth mode shape in x, y and z direction; $P_{ix}(t)$, $P_{iy}(t)$ and $P_{iz}(t)$ are dynamic force acting on the ith floor of the building in x, y and z directions.

4.2.1 Generalized Displacement Response

Generalized displacement uses the generalized wind force to calculate the solution of the equation of motion in each vibration mode according to structural dynamics. This can be calculated using the equations below, which were proposed by Chen and Kareem (2005b).

$$\bar{q}_j = \frac{\bar{Q}_j}{K_j} \tag{13},$$

$$\sigma_{q_{jb}}^2 = \frac{1}{K_j{}^2}\int_0^\infty S_{Q_{jj}}(f)\,df \tag{14},$$

$$\sigma_{q_{jr}}^2 = \frac{1}{K_j{}^2}\frac{\pi}{4\xi_j} f_j S_{Q_{jj}}(f_j) \tag{15},$$

$$K_j = (2\pi f_j)^2 \sum_{k=1}^{N}\left(m_i\phi_{ijx}^2 + m_i\phi_{ijy}^2 + I_i\phi_{ijz}^2\right) \tag{16},$$

$$\sigma_{q_j} = \sqrt{\sigma_{q_{jb}}^2 + \sigma_{q_{jr}}^2} \tag{17},$$

where $\bar{q}_j$, $\sigma_{q_{jb}}^2$ and $\sigma_{q_{jr}}^2$ are mean, root-mean-square background and resonant of the generalized displacement of jth mode; σ_{q_j} is the dynamic generalized displacement of jth mode; K_j, f_j and ξ_j are generalized stiffness, generalized frequency and generalized damping of jth mode; m_i and I_i are mass and mass moment of inertia of the ith floor; $S_{Q_{jj}}$ is power spectrum density of $Q_j(t)$.

4.2.2 The Modal Correlation Coefficients between Two Response

The modal correlation coefficients between the jth and kth dynamic modal responses are

$$r_{jk} = \frac{\sigma_{q_{jk}}}{\sigma_{q_j}\sigma_{q_k}} = \frac{r_{jkb}\sigma_{q_{jb}}\sigma_{q_{kb}} + r_{jkr}\sigma_{q_{jr}}\sigma_{q_{kr}}}{\left(\sqrt{\sigma_{q_{jb}}{}^2 + \sigma_{q_{jr}}{}^2}\right)\left(\sqrt{\sigma_{q_{kb}}{}^2 + \sigma_{q_{kr}}{}^2}\right)} \tag{18},$$

where r_{jk}, r_{jkb} and r_{jkr} are modal correlation coefficients of the jth and kth dynamic, background and resonance modal responses, respectively.

4.2.3 Resultant Response

The standard deviation of the generalized displacement can be used to calculate the standard deviation of any interesting response in the jth mode of vibration using

$$\Gamma_j = \sum_{i=1}^{n}\left(2\pi f_j\right)^2\left(m_i\phi_{ijx} + m_i\phi_{ijy} + I_i\phi_{ijz}\right) \tag{19},$$

$$\sigma_{R_j} = \Gamma_j\sigma_{q_j} \tag{20},$$

where σ_{R_j} is the resultant response of interest in the jth mode; Γ_j is jth modal participation coefficient.

4.2.4 Weighting Factor

The weighting factor is the function of the ratio of the modal response component and the modal correlation coefficients. Which W_{1R} maximum is using the Equations (22) and (23), and W_{2R} maximum is using the Equations (25) and (26). The following combination can be defined (Chen and Kareem, 2005b).

$$W_{1R}^{(1)} = 1 \tag{21}$$

$$W_{2R}^{(1)} = \left[\sqrt{1+\left(\sigma_{R_2}/\sigma_{R_1}\right)^2 + 2r_{12}\left(\sigma_{R_2}/\sigma_{R_1}\right)} - 1\right]\left(\sigma_{R_1}/\sigma_{R_2}\right) \tag{22}$$

$$W_{3R}^{(1)} = \left[\sqrt{1+\left(\sigma_{R_3}/\sigma_{R_1}\right)^2 + 2r_{13}\left(\sigma_{R_3}/\sigma_{R_1}\right)} - 1\right]\left(\sigma_{R_1}/\sigma_{R_3}\right) \tag{23}$$

$$W_{2R}^{(2)} = 1 \tag{24}$$

$$W_{1R}^{(2)} = \left[\sqrt{1+\left(\sigma_{R_1}/\sigma_{R_2}\right)^2 + 2r_{12}\left(\sigma_{R_2}/\sigma_{R_1}\right)} - 1\right]\left(\sigma_{R_2}/\sigma_{R_1}\right) \tag{25}$$

$$W_{3R}^{(2)} = \left[\sqrt{1+\left(\sigma_{R_3}/\sigma_{R_2}\right)^2 + 2r_{13}\left(\sigma_{R_3}/\sigma_{R_2}\right)} - 1\right]\left(\sigma_{R_2}/\sigma_{R_3}\right) \tag{26}$$

When $\sigma_{R_1} = \sigma_{R_2} = \sigma_{R_3}$, Equations (22), (23) , (25) and (26) lead to

$$W_{2R}^{(1)} = W_{1R}^{(2)} = \sqrt{2+2r_{12}} - 1 \tag{27}$$

$$W_{3R}^{(1)} = \sqrt{2+2r_{13}} - 1 \tag{28}$$

$$W_{3R}^{(2)} = \sqrt{2+2r_{23}} - 1 \tag{29}$$

which is comparable to the combination rule approved by AIJ 2004 that takes into consideration modal correlation. By further setting $r_{12} = r_{13} = 0$ and $r_{23} = 0.2$, it leads to $W_{2R}^{(1)} = W_{1R}^{(2)} = W_{3R}^{(1)} \approx 40\%$ and $W_{3R}^{(2)} \approx 0.55$, i.e., the 40% rule, which has been widely used in wind load combination in building standards as shown in Table 1.

Table 1: Wind load combinations for high-rise buildings in AIJ 2004 standard.

Combination	Along-wind load	Across-wind load	Torsional load
1	$M_{\max}$	$\bar{M} + 0.4M_{dyn}$	$\bar{M} + 0.4M_{dyn}$
2	$\bar{M} + 0.4M_{dyn}$	$M_{\max}$	$\bar{M} + 0.55M_{dyn}$
3	$\bar{M} + 0.4M_{dyn}$	$\bar{M} + 0.55M_{dyn}$	$M_{\max}$

4.2.5 Equivalent Static Wind Loads

The mean and dynamic equivalent static load can be calculated from the mean and dynamic generalized displacement from the following relationship.

$$\bar{F}_{ijs} = \left(2\pi f_j\right)^2 m_{is}\phi_{ijs}\bar{q}_j \qquad (s = x, y, z) \tag{30},$$

$$\bar{F}_{mean} = \bar{F}_{i1s} + \bar{F}_{i2s} + \bar{F}_{i3s} \tag{31},$$

$$F_{ijs} = \left(2\pi f_j\right)^2 m_{is}\phi_{ijs} g\sigma_{q_j} \qquad (s = x, y, z) \tag{32},$$

$$F_{dyn} = W_{1R}F_{i1s} + W_{2R}F_{i2s} + W_{3R}F_{i3s} \tag{33},$$

$$F_{total} = F_{mean} \pm F_{dyn} \tag{34},$$

$$g = \sqrt{2\ln(fT)} + 0.5772 / \sqrt{2\ln(fT)} \tag{35},$$

where $\bar{F}_{ijs}$, F_{ijs} and F_{total} are mean, dynamic and total equivalent static wind load acting on the mass center of the ith floor in s direction; g is peak factor. The resultant base moments are obtained by summing the equivalent static wind loads by the moment arms.

5 Result and Discussion

5.1 Comparison between HFFB and HFPI by the Base Moment Analysis

The mean wind force coefficients in x and y directions are shown in Figure 6(a-b) as a function of the approaching wind direction. It can be observed that C_x is high at 0 and 180 degrees, which M_y is an along-wind base moment. For C_y is high at 90 and 270 degrees, which M_x is an along-wind moment. In the along-wind direction, most of the wind effects are those that hit the building directly, this is relatively smooth and has low fluctuation. Both HFFB and HFPI provide results that are consistent with the physical definitions for building responses under wind loads according to previous studies (Steckley et al., 1992; Zhou et al., 2003; Kwon et al., 2008). From Figure 6(c), it can be seen that C_z the HFPI is smoother than HFFB due to the effect of the imperfection of the model, and C_z the HFPI approaches zero at every 45 degrees, which corresponds to the physical definition. As for HFFB, only the angle range 130 to 210 produces inconsistent results. However, C_z both tests tend to increase and decrease in the same direction.

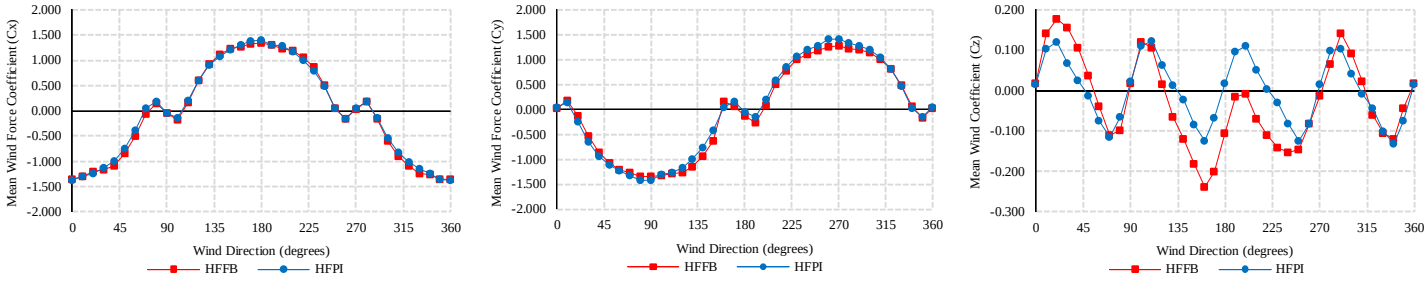

(a) (b) (c)

Figure 6: Mean wind force coefficients: (a) x-direction (b) y-direction (c) z-direction

RMS base moment coefficients of M_x, M_y and M_z with respect to wind direction are shown in Figure 7(a-c). It can be observed that RMS of M_x is high at 0 and 180 degrees, which M_x is the across-wind base moment. RMS M_y is high at 90 and 270 degrees, which M_y is the across-wind base moment. For across-wind direction, most of the wind effect on the building is from the turbulent nature of wind, which is the vortex shedding. The results of both HFFB and HFPI are compatible with the physical criteria. Figure 7(c) shows that RMS M_z for the HFPI is smoother than the HFFB because of the model's imperfection. Nevertheless, RMS M_z for both tests tends to increase and decrease in the same directions.

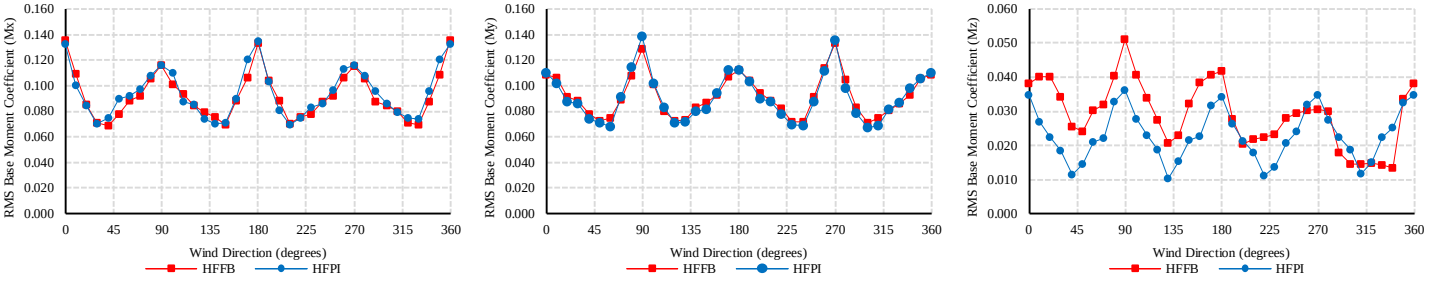

(a) (b) (c)

Figure 7: RMS base moment coefficients: (a) Mx (b) My (c) Mz.

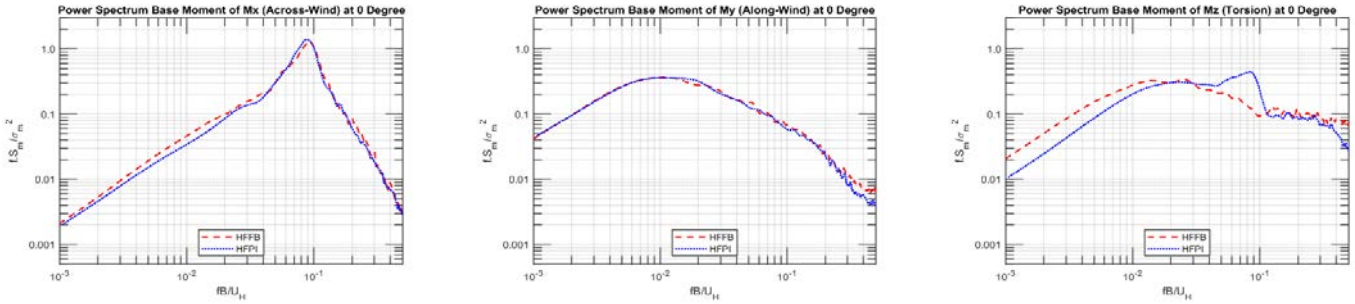

(a) (b) (c)

Figure 8: Power spectrum density (PSD) at 0-degree wind direction of (a) Mx (b) My (c) Mz

Figure 8(a-c) provides the power spectrum density (PSD) at 0 degrees, it can be seen that the PSD of M_x (Across-wind) for the HFFB and HFPI test are approximately the same with a dominant amplitude at $fB/U_H \approx 0.1$ (Strouhal frequency number). The PSD of M_y (Along-wind) for the HFFB and HFPI tests are nearly identical. Figure 8 also illustrates the corresponding range of results from other studies (Steckley et al., 1992; Zhou et al., 2003; Kwon et al., 2008). The PSD M_z for HFFB and HFPI tests are quite similar, but HFFB is higher in some frequencies.

Base moments of the real building about x, y and z axis in terms of mean, background and resonance are shown in Figure 9(a-c) as a function of the approaching wind direction. The results obtained are consistent with the non-dimensional aerodynamic coefficients described previously. The HFFB and HFPI test produce similar results in both the mean, background and resonance parts. From Table 2, it can be seen that the base moment about the x-axis in the mean, background, resonance and total are different by 8%, 2%, 5% and 3%, respectively. The mean, background, resonance and total base moments about the y-axis varied by 2%, 1%, 2% and 1%, respectively. The base moment about the z-axis is significantly different from the imperfection of the model. The

mean, background, resonance and total differ by 30%, 17%, 33% and 26%, respectively.

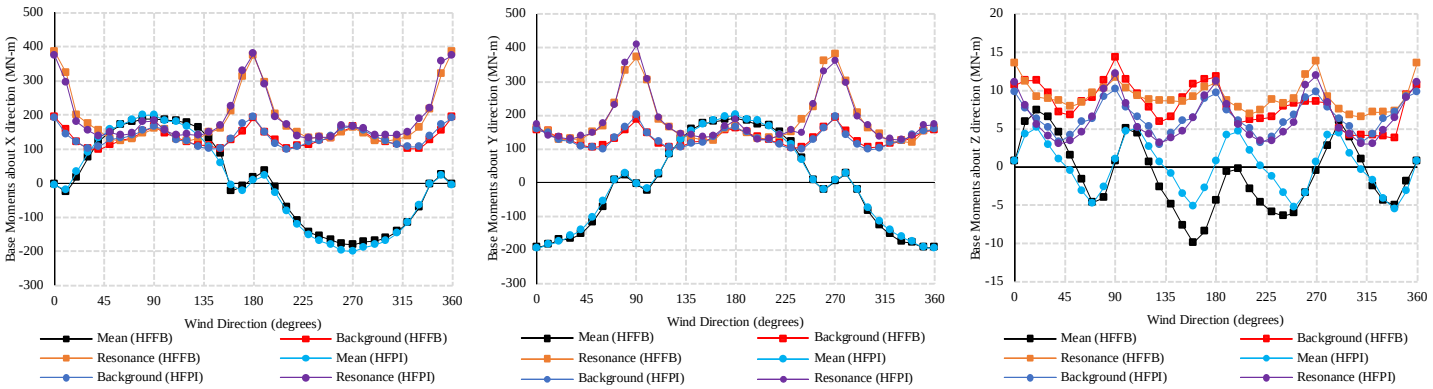

(a) (b) (c)

Figure 9: Base moments of the real building about: (a) x-direction (b) y-direction (c) z-direction

Table 2: The average results of comparing the base moments of real buildings between the HFFB and HFPI.

Average	HFPI/HFFB			
	Mean	Background	Resonance	Total
The base moment about X-axis	1.08	1.02	1.05	1.03
The base moment about Y-axis	0.98	0.99	1.02	0.99
The base moment about Z-axis	1.37	0.83	0.67	0.74

5.2 The Results of Modal Correlation Coefficient and Weighting Factor

The modal correlation coefficient between the two modes is shown in Figure 10(a-c) as a function of the approaching wind direction. It can be observed that the predictions from the HFFB and HFPI tests generally have good agreement. The modal correlation between 1th and 2th modal (x and y direction) is not always equal to zero, the positive and negative peak correlations for the HFFB are between 0.1 and -0.19, and are between 0.175 and -0.178 for the HFPI. The modal correlation between 2th and 3th modal (y and z direction) for the HFFB has positive and negative peaks correlations that are between 0.31 and -0.23, and between 0.33 and -0.34 for the HFPI. The 1th and 3th modal (x and z direction) have positive and negative peaks correlations than are between 0.43 and -0.03 for the HFFB, and 0.34 and -0.38 for the HFPI.

Figure 11(a-b) shows the weighting factor that takes into consideration the modal correlation coefficient as a function of the approaching wind direction in the case of W_{1R} maximum (M_y is max) and W_{2R} maximum (M_x is max), respectively. Results obtained from the HFFB show close agreement with the HFPI. It can be seen that the weighting factor for the case of W_{1R} maximum, W_{2R} is higher than AIJ 2004 standard at 0 and 180 degrees (M_x=across-wind and M_y =along-wind), and lower than AIJ 2004 at 90 and 270 degrees (M_x=along-wind and M_y=across-wind). In the case of W_{2R} maximum, W_{1R} is lower than AIJ 2004 standard at 0 and 180 degrees, and higher than AIJ 2004 at 90 and 270 degrees. For the case of W_{1R} and W_{2R} are maximum, W_{3R} is less than AIJ 2004 in all of the angles of attack.

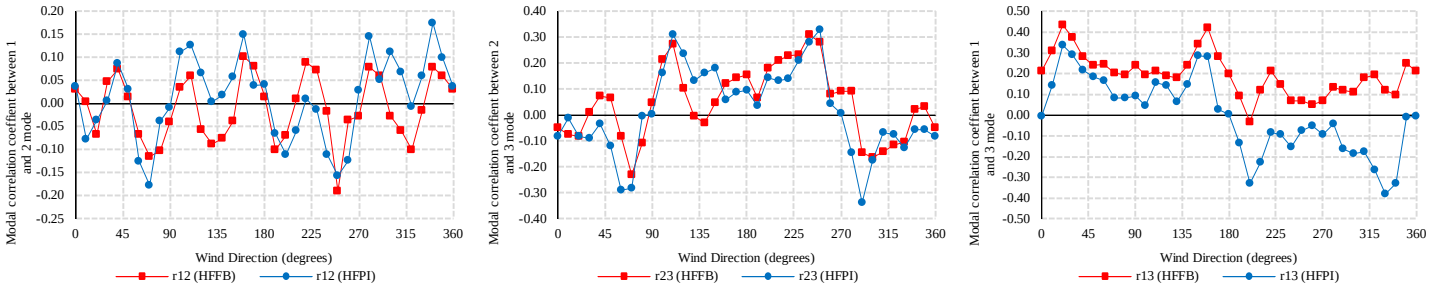

(a) (b) (c)

Figure 10: The modal correlation coefficients between (a) 1th and 2th modes (b) 2th and 3th modes (c) 1th and 3th modes

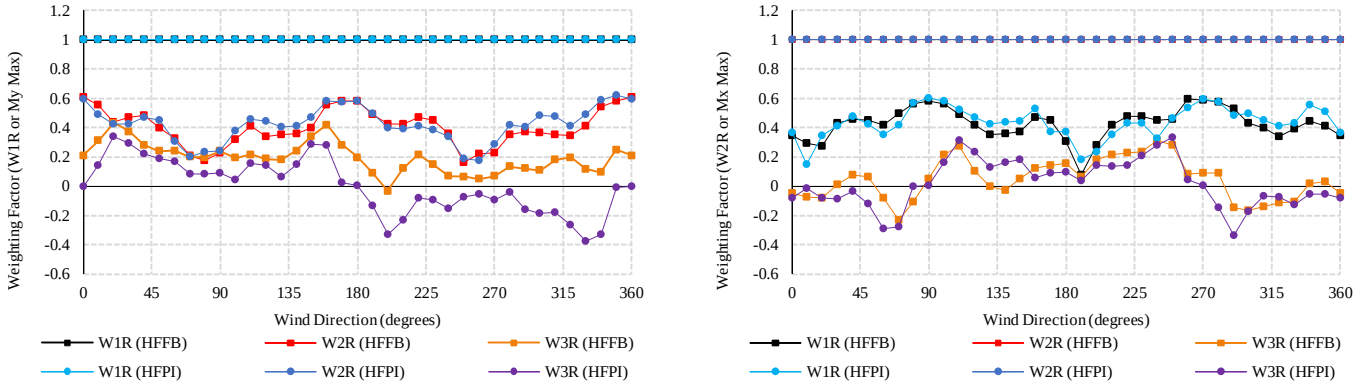

(a) (b)

Figure 11: The weighting factors in case of (a) W_{1R} or My maximum (b) W_{2R} or Mx maximum

5.3 Wind Load Combination between Weighting Factor and AIJ 2004

The wind load combinations of base moments for the HFPI by weighting factor and AIJ 2004 standard are shown in Figure 12(a-c) with respect to wind direction. The resultant base moments are obtained by summing between mean and dynamic base moments.

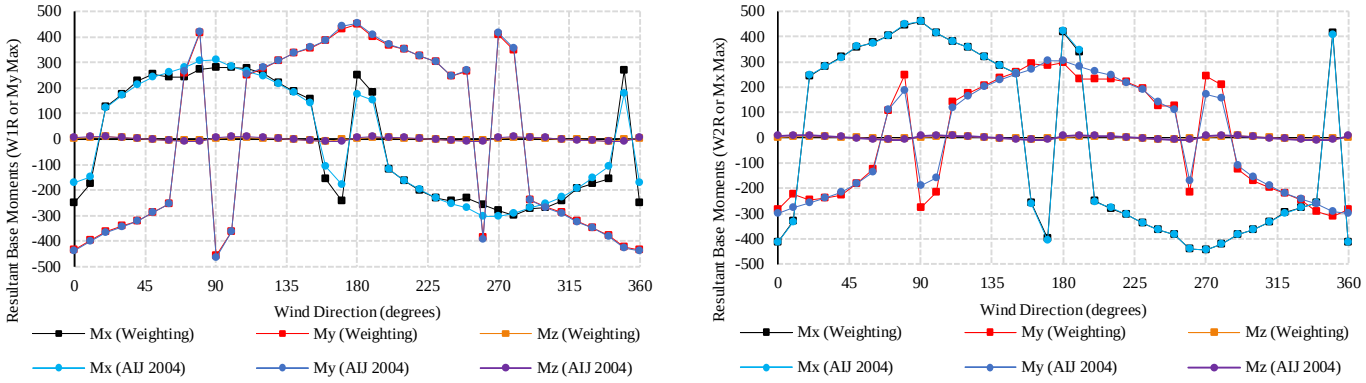

(a) (b)

Figure 12: The resultant base moments in case of (a) W_{1R} or My max (b) W_{2R} or Mx max

The percent difference of wind load combinations is illustrated in Tables 3 and 4, which show the difference of the resultant base moments from the combination by a weighting factor and AIJ 2004 at critical wind direction for the buildings with an aspect ratio of width to depth equal to 1. It can be seen that in the case of along-wind maximum, the combination of across-wind by AIJ 2004 is less than the weighting factor of 32%, 30%, 31% and 30%, which the average is 31%. In the case of across-wind maximum, the combination of along-wind by AIJ 2004 can be observed to be higher

than the weighting factor of 12%, 8%, 5% and 3%, which the average is 7%. For the combination of torsional, the result indicated that the AIJ 2004 standard produced significantly higher results than the weighting factor in all of the cases.

Table 3: The resultant base moments of real buildings from the combination of the weighting factor (A) and AIJ 2004 standard (B) in case of W_{1R} or My max.

Degree	Along-wind	Across-wind	W_{1R} or My maximum (MN m)								
			Mx			My			Mz		
			(A)	(B)	(B)/(A)	(A)	(B)	(B)/(A)	(A)	(B)	(B)/(A)
0	My	Mx	-250	-170	0.68	-434	-438	1.01	0.65	6.57	10.09
90	Mx	My	279	311	1.12	-457	-465	1.02	2.38	7.50	3.15
180	My	Mx	249	174	0.70	451	452	1.00	0.87	6.80	7.80
270	Mx	My	-282	-304	1.08	409	414	1.01	2.00	6.63	3.33

Table 4: The resultant base moments of real buildings from a combination of the weighting factor (A) and AIJ 2004 standard (B) in case of W_{2R} or Mx max.

Degree	Along-wind	Across-wind	W_{2R} or Mx maximum (MN m)								
			Mx			My			Mz		
			(A)	(B)	(B)/(A)	(A)	(B)	(B)/(A)	(A)	(B)	(B)/(A)
0	My	Mx	-412	-415	1.01	-286	-300	1.05	1.84	6.57	3.56
90	Mx	My	462	459	0.99	-275	-190	0.69	0.98	7.50	7.66
180	My	Mx	417	422	1.01	297	305	1.03	2.25	6.80	3.03
270	Mx	My	-443	-443	1.00	244	171	0.70	0.63	6.63	10.57

6 Conclusion

This study's findings validated some of the conclusion of prior studies that used the HFFB and HFPI tests, as well as provided some new results that helped to better understand and quantify the wind-induced loads of tall buildings. The results indicate that the HFFB and HFPI tests can give similar results for the overall wind loads, modal correlation coefficient and weighting factor.

For tall buildings with an aspect ratio of width to depth equal to 1.0, the combination of across-wind load, where the maximum along-wind direction according to AIJ 2004 is lower than the combination by a weighting factor, which means an underestimation of the response. This is because AIJ 2004 is based on non-correlation between along and across-wind and assumes that the along-wind load is equal to the across-wind load. In fact, the modal correlation coefficient between along and across is not always zero.

For the combination of along-wind load, where the maximum across-wind direction according to AIJ 2004 is higher than the combination by a weighting factor, which means conservative. In the case of the along- and across-wind maximum, the combination of torsional loads according to AIJ 2004 is greater than the combination by a weighting factor, which denotes a very conservative. Because of the buildings with an aspect ratio of 1.0, the torsional response is quite minimal in comparison to the along-wind and across-wind responses, which means a small ratio of modal response, resulting in the weighting factor for combination in the torsional direction being very lower than AIJ 2004 standard.

7 Availability of Data and Material

Data can be made available by contacting the corresponding author.

8 Acknowledgement

The authors are grateful for the financial support from Thammasat School of Engineering, Thammasat University, Thailand.

9 References

AIJ (2004). *Recommendations for load on buildings*. Architectural Institute of Japan, C6-63-65.

Andrew Steckley, Marco Accardo, Scott L. Gamble and Peter A. Irwin. (1992). The Use of Integrated Pressure to Determine Overall Wind-induced Response. *Journal of Wind Engineering and Industrial Aerodynamics*, 1023-1034.

Asami, Y. (2000). Combination method for wind loads on high-rise buildings. *Proceeding 16th National Symp. On Wind Engineering*. Japan Association for Wind Engineering JAWE, Tokyo, 531-534.

Dae Kun Kwon, Seymour M.J. Spence and Ahsan Kareem. (2014). A Cyberbased Data-Enabled Design Framework for High-rise Buildings Driven by Synchronously Measured Surface Pressures. *Advances in Engineering Software*, 13-27.

Dae-Kun Kwon, Tracy Kijewski-Correa and Ahsan Kareem. (2008). E-analysis of High-Rise Buildings Subjected to Wind Loads. *Journal of Structural Engineering*, 1139-1153.

Xinzhong Chen and Ahsan Kareem. (2005a). Coupled dynamic analysis and equivalent static wind loads on buildings with three-dimensional modes. *Journal of Engineering Mechanics*, 1071-1082.

Xinzhong Chen and Ahsan Kareem. (2005b). Dynamic Wind Effects on Buildings with 3D Coupled Modes. *Journal of Engineering Mechanics*, 1115-1125.

Yin Zhou, Tracy Kijewski and Ahsan Kareem. (2003). Aerodynamic Loads on Tall Buildings: *Interactive Database. Journal of Structural Engineering*, 394-404.

Yukio Tamura, Hirotoshi Kikuchi, and Kazuki Hibi. (2003). Quasi-static Wind Load Combinations for Low and Middle-rise Buildings. *Journal Wind Engineering and Industrial Aerodynamics*, 1613-1625.

Yukio Tamura, Yong Chul Kim, Hirotoshi Kikuchi and Kazuki Hibi. (2013). Correlation and Combination of Wind Force Components and Response. *Journal of Wind Engineering and Industrial Aerodynamics*, 81-93.

Wasin Thangthong is a Master's degree student at the Department of Civil Engineering, Thammasat University, Thailand. He earned a Bachelor of Engineering (Civil Engineering and Management) from Thammasat University, Thailand. He is interested in Evaluation Wind Load and Response to Structure.

Dr. Virote Boonyapinyo is an Associate Professor at Thammasat University Thailand. He earned a Bachelor's degree from Chulalongkorn University, Thailand, a Master's degree in Structural Engineering from Chulalongkorn University, Thailand, and a Ph.D. in Structural Engineering from Yokohama National University, Japan. He is interested in Structure Dynamics, Evaluation of Wind and Earthquake Loads on Structure, Wind Tunnel Tests, Long-span Bridges and High-Rise Buildings.

Dr. Jirawat Junruang is a Lecturer at Rajamangala University of Technology Tawan-ok(Uthenthawai Campus), Thailand. He received his B.Eng. from King Mongkut's University of Technology North Bangkok. He got a Master's and a Ph.D. in Structural Engineering from Thammasat University, Thailand. He is interested in the Evaluation of Wind and Earthquake Loads on Structure, Wind Tunnel Tests and Computational Fluid Dynamic (CFD).